

# Effect of synthesis route on the uptake of Ni and Cd by $\text{MgFe}_2\text{O}_4$ nanopowders

B. Al-Najar<sup>1</sup> · L. Khezami<sup>2</sup> · J. Judith Vijaya<sup>3</sup> · O. M. Lemine<sup>4</sup> · M. Bououdina<sup>1</sup>

Received: 8 October 2016 / Accepted: 15 December 2016 / Published online: 28 December 2016  
© Springer-Verlag Berlin Heidelberg 2016

**Abstract** In this study,  $\text{MgFe}_2\text{O}_4$  nanopowders were synthesized through two different methods, sol–gel method (SG) and modified sol–gel with Ammonia (MSG-A). The influence of synthesis route was investigated in terms of phase stability, pores size and surface area, magnetic properties and uptake of Ni and Cd metals from aqueous solution. Rietveld refinements of x-ray diffraction patterns confirmed the formation of single spinel phase for SG sample, while minor impurity was detected for SGM-A sample (few amount of  $\text{MgO}$ ). The crystallite size was found to be sensitive to the preparation method; it ranges from 4 nm for SG to 15 nm for MSG-A. Magnetization experiment at room temperature showed ferromagnetic behavior with a saturation magnetization ( $M_s$ ) ranging from 5.39 emu/g for SG to 9.93 emu/g for MSG-A. Preliminary results showed that SG and MSG-A samples are efficient adsorbent for Ni and Cd metal ions from aqueous solution. Maximum quantity of 62.67 and 61.2 mg of Ni(II) and 36.49 and 32.84 mg of Cd(II) was adsorbed per gram of  $\text{MgFe}_2\text{O}_4$  synthesized by SG and MSG-A, respectively.

## 1 Introduction

Nanoparticles (NPs) have been used widely in modern biotechnology and environmental applications due to their benefits upon bulk materials. NPs have shown to own interesting adsorption efficiency; hence, they have been used to clean wastewater from pollutant such as heavy metals. Studies revealed that iron oxides are very important NPs adsorbents as they have shown interesting efficiency in the adsorption of Ag, Hg, Mn, Zn, Pb and Cd ions from waste water [1]. Other polymeric NPs were applied successfully in the adsorption of Hg, Pb and Cd [2].

Among nanomaterials, spinel ferrites with the general formula  $\text{AFe}_2\text{O}_4$  ( $A = \text{Mn, Co, Ni, Mg or Zn}$ ) have unique optical, electric, magnetic and chemical properties. Their small size, low cost, high stability and environmental friendly offer numerous environmental applications [3]. Recently, synthesized spinel ferrites NPs including  $\text{MgFe}_2\text{O}_4$  have shown high removal efficiency of chromium (Cr) which is a toxic pollutant present in aqueous systems. It was also shown that this efficiency varies with the magnetic properties of  $\text{MgFe}_2\text{O}_4$  NPs [4] which depends in turns in their synthesis route. Other studies demonstrated that  $\text{MgFe}_2\text{O}_4$  NPs were efficient in the removal of some environmental pollutant such as  $\text{SO}_2$  in atmosphere [5] and arsenic (As) in drinking water [3].

A broad variety of methods are being applied to synthesize magnesium ferrite ( $\text{MgFe}_2\text{O}_4$ ) including combustion [6], electrospinning [7, 8], thermal treatment [9], solvothermal route [10], micro-emulsion [11] and chemical co-precipitation [12, 13]. It is well known that the synthesis route as well as the starting precursors reagents and post-annealing control the shape, particle size, agglomeration and chemical composition (deviation from stoichiometry which creates structural defects such as vacancies).

✉ B. Al-Najar  
balnajar85@gmail.com

<sup>1</sup> Department of Physics, College of Science, University of Bahrain, PO Box 32038, Sakhir, Kingdom of Bahrain

<sup>2</sup> Department of Chemistry, College of Sciences, Al Imam Mohammad Ibn Saud Islamic University, Riyadh, Saudi Arabia

<sup>3</sup> Catalysis and Nanomaterials Research Laboratory, Department of Chemistry, Loyola College, Chennai 600034, Tamil Nadu, India

<sup>4</sup> Department of Physics, College of Sciences, Al Imam Mohammad Ibn Saud Islamic University, Riyadh, Saudi Arabia

Therefore, different approaches of synthesis may vary considerable properties of NPs. For example, in electro-spinning method,  $\text{Mg}(\text{NO}_3)_2 \cdot 6\text{H}_2\text{O}$ ,  $\text{Fe}(\text{NO}_3)_3 \cdot 9\text{H}_2\text{O}$ , PVP, DMF, acetic acid and ethanol have been used as starting chemicals to prepare  $\text{MgFe}_2\text{O}_4$  nanofibers [7]. The results showed that the saturation magnetization  $M_s$  at room temperature ranges from 17.0 emu/g after calcination at 500 °C to 31.1 emu/g after calcination at 800 °C.

However, some other approaches lead to lower values in saturation magnetization. A thermal treatment method was applied on very similar starting chemicals ( $\text{Fe}(\text{NO}_3)_3 \cdot 9\text{H}_2\text{O}$ ,  $\text{Mg}(\text{NO}_3)_2 \cdot 6\text{H}_2\text{O}$  and PVA) gave a maximum saturation magnetization of the synthesized  $\text{MgFe}_2\text{O}_4$  nanocrystals calcined at 973 K of 11.74 emu/g. The authors related this low value to the existence of inactive magnetic layer on the surface of NPs [9]. Recently, micro-emulsion was applied to prepare  $\text{MgFe}_2\text{O}_4$  NPs [11], and the saturation magnetization was found even lower (9.84 emu/g) which was associated to the speculated differences in inversion parameter and redistribution of Mg ions among A and B sites of the spinel structure.

The aim of this research work is to investigate the effect of synthesis route [sol–gel (SG) and modified sol–gel using ammonia (MSG-A)] and starting precursors on the phase stability, microstructure and magnetic properties of  $\text{MgFe}_2\text{O}_4$  nanopowders. Structure, microstructure, magnetic and surface properties were analyzed. Furthermore, an evaluation of the efficiency of these products for the removal of various metals ions (Cd(II) and Ni(II)) from aqueous solution has been performed.

## 2 Experimental part

### 2.1 Preparation of $\text{MgFe}_2\text{O}_4$ nanopowders

$\text{MgFe}_2\text{O}_4$  nanopowders were prepared using two synthesis approaches sol–gel (SG) and modified sol–gel using ammonia (MSG-A). Both methods were followed by calcination at 500 °C. The synthesis steps for each method are discussed (detailed) below:

#### 2.1.1 Sol–gel (SG) method

Calculated amounts of magnesium nitrate and ferric nitrate were dissolved in double-deionized water followed by adding citric acid as a gelling agent. Then stirring was applied to the solution resulting at room temperature for 1 h until a clear transparent solution was obtained. This clear solution was kept for gellation at 65 °C for 12 h, and the gel was then dried at 110 °C, followed by calcination at 500 °C for 2 h (Fig. 1a).

#### 2.1.2 Modified sol–gel method with ammonia (MSG-A)

Calculated amounts of magnesium nitrate and ferric nitrate were dissolved in double-distilled water followed by adding citric acid as a gelling agent. Then stirring was applied at room temperature for half an hour until a clear transparent solution was obtained, and ammonia was added in order to adjust the pH value to 10. Then the resultant solution was kept under heat of 100 °C and constant stirring for 1 h. The obtained powders were subsequently calcined at 500 °C with a heating rate of 5 °C/min for 2 h under atmosphere air flow (Fig. 1b).

### 2.2 Characterization of $\text{MgFe}_2\text{O}_4$ nanopowders

Phase analysis of  $\text{MgFe}_2\text{O}_4$  nanopowders was attained by X-ray diffraction (XRD) measurement using high-resolution Rigaku Ultima IV diffractometer equipped with Cu-K  $\alpha$  radiation ( $\lambda_{k\alpha} = 1.5418 \text{ \AA}$ ). Qualitative and quantitative phase analysis was achieved using PDXL program. The refinements were carried out using  $\text{MgFe}_2\text{O}_4$  spinel phase with a cubic crystal structure (space group Fd3m; No. 227), Fe metal with cubic crystal structure (space group Fm3m, No. 227), and MgO with cubic structure (space group Fm3m No. 225). The refinements included phase composition, lattice parameters and microstructural parameters (crystallite size and microstrain). The morphology of the nanopowders has been investigated by field emission scanning microscope (FESEM) using JEOL-JSM-7600F equipped with energy-dispersive spectroscopy (EDS). Magnetization-field (M-H) hysteresis loops of the as-prepared powders were measured at room temperature using PMC MicroMag 3900 model vibrating sample magnetometer (VSM) having a 1-Tesla magnet and a sensitivity of 0.5  $\mu\text{emu}$ .

The specific surface areas,  $S_{\text{BET}}$ , were estimated using the BET (Brunauer–Emmett–Teller) method. The total pore volume of micropores and surface areas of mesopores were calculated from the t-plot method of Lippens and de Boer [14]. The pore size distribution (PSD) was determined by the BJH (Barrett–Joyner–Halenda) method applied on the adsorption–desorption hysteresis loop [15].

The  $\text{N}_2$  adsorption–desorption isotherms of the  $\text{MgFe}_2\text{O}_4$  nanopowders were measured at 77 K using an automatic adsorption analyzer (ASAP 2020, Micromeritics). The SG and MSG-A samples were degassed under vacuum at 100 °C for about 2 h prior to each measurement.

### 2.3 Adsorption experiments

Ni(II) and Cd(II) stock solutions (1000 mg/L) were prepared in distilled water using nickel nitrate ( $\text{Ni}(\text{NO}_3)_2$ ) and

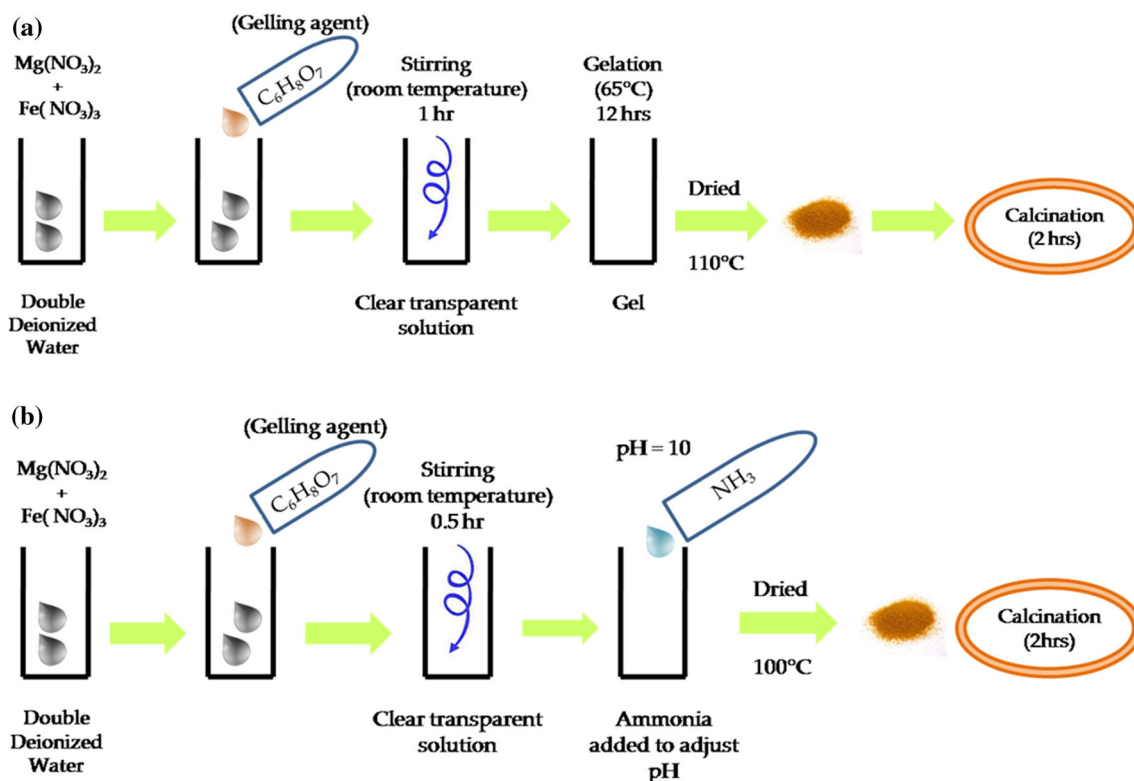


**Fig. 1** Synthesis steps of MgFe<sub>2</sub>O<sub>4</sub> nanopowders via **a** Sol-gel method **b** modified sol-gel with ammonia

cadmium nitrate (Cd(NO<sub>3</sub>)<sub>2</sub>). Successive dilutions were then applied to the experimental solutions in order to obtain the desired concentration. All the reagents were of analytical grade or highest purity available and used without further purification. The experiments were conducted in batch mode by adding 16 mg of MgFe<sub>2</sub>O<sub>4</sub> powders obtained by MSG-A and SG to 25 ml of different metal ion solution having different initial concentrations with a pH fixed at about  $7.0 \pm 0.2$  at room temperature in a 50-ml conical flask.

The initial concentrations of Ni(II) and Cd(II) are 40.2 and 68.85 mg/L, respectively. The mixtures were stirred by a magnetic stirrer (600 rpm) for 12 h according to our preliminary tests. 15 ml of suspension is sampled from each flask and filtered using 0.25- $\mu$ m cellulose acetate syringe filters and then centrifuged at 6000 rpm for 10 min. The concentrations of Ni(II) and Cd(II) in the filtrate are measured by inductively coupled plasma-atomic emission spectrometry. The amount of adsorbed solute  $q_e$  was determined as follows:

$$q_e = \frac{(C_0 - C_e) * V}{m} \quad (1)$$

where  $C_0$  and  $C_e$  are the initial and equilibrium concentrations, respectively ( $\text{mg.l}^{-1}$ ),  $V$  the volume of the pollutant solution (l) and  $m$  the mass of the nanopowder (mg).

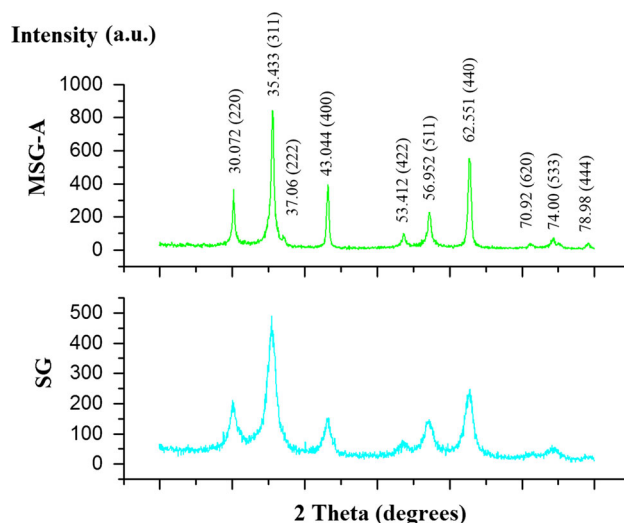


**Fig. 2** X-ray diffraction patterns of MgFe<sub>2</sub>O<sub>4</sub> nanopowders prepared by SG and MSG-A methods

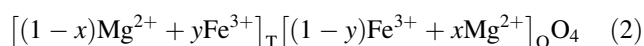
## 3 Results and discussion

### 3.1 Structural and morphological characteristics

X-ray diffraction patterns of the calcined MgFe<sub>2</sub>O<sub>4</sub> nanopowders are shown in Fig. 2. All the main peaks are indexed using spinel cubic MgFe<sub>2</sub>O<sub>4</sub> phase. The calculated

crystallite size (CS) ranges from 4 up to 13 nm for nanopowder calcined at 500 °C. No additional peaks corresponding to other phases were observed in XRD patterns for nanopowder prepared by SG. However, for nanopowders prepared by MSG-A, additional peaks corresponding to other phases were observed, indicating the presence of some impurities of MgO (18%).

The refined values of the lattice parameter reported in Table 1 for both SG and MSG-A samples are close to the value of the spinel  $\text{MgFe}_2\text{O}_4$  phase reported in the literature [9]. Meanwhile, the lattice parameter of MSG-A is slightly higher than of SG. This can be associated with metal ion redistribution among tetrahedral and octahedral ionic sites [16], in accordance with ionic radii ( $r(\text{Mg}^{2+}) = 0.72 \text{ \AA}$ ,  $r(\text{Fe}^{3+}) = 0.64 \text{ \AA}$ ):



FESEM images for  $\text{MgFe}_2\text{O}_4$  nanopowders showed agglomerated grains distributed non-uniformly with size ranging from 5 to 30 nm for SG sample (Fig. 3a) and 20 to 50 nm for MSG-A sample (Fig. 3b). Such agglomeration has been found in many cases of  $\text{MgFe}_2\text{O}_4$  NPs prepared by chemical routes [9, 17, 18], which is due to the natural interactions between these magnetic NPs (each NP acts as magnet) [9] and to their high surface energy [18]. FESEM images also confirm that adding ammonia as a modifier during synthesis in sol-gel method (MSG-A) results in larger particles size, which agree with XRD results (Table 1).

This can be explained as the presence of ammonium ions in the reaction medium has a twofold role; it alters the pH of the medium and reduces the amount of the energy required to start the nucleation or in other words enhances the rate of nucleation. Therefore, if the concentration of ammonia is increased, the number of active groups at the surface of NPs will increase too and, hence, favor the aggregation of the particles into larger ones. Moreover, the addition of amine-based compounds like ammonia retards the growth of bulk  $\text{MgFe}_2\text{O}_4$  phase because of its property of strong coordination interaction with metal ions, leading to an increase in the surface area and enhancement in porosity [19–23].

The magnetization-field (M-H) curves of the calcined  $\text{MgFe}_2\text{O}_4$  nanopowders obtained from room temperature

VSM measurements are shown in Fig. 4. The magnetization-field (M-H) curves show the presence of room temperature ferromagnetism (RTFM) with a small paramagnetic component, which was removed to obtain the correct values of saturation magnetization reported in Table 1. The M-H curves correspond to a soft magnetic material and indicate ferromagnetism with a hysteresis loop in the field range of  $\pm 5000 \text{ Oe}$ , while outside this range, the magnetization is proportional to the applied magnetic field and reaches saturation in the investigated field range of ( $\pm 10 \text{ kOe}$ ). According to the results (Table 1),  $M_s$  ranges from 5.4 to 9.9 emu/g. Fe ions were not identified in both samples, and hence, the resulted magnetization is considered to be due the spinel phase of

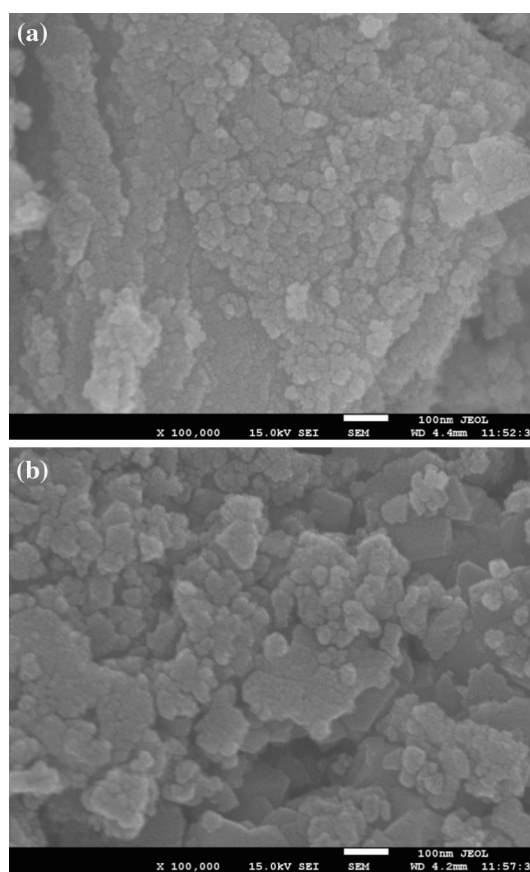


**Fig. 3** FESEM images for  $\text{MgFe}_2\text{O}_4$  nanopowders prepared by **a** sol-gel method (SG) **b** modified sol-gel method with ammonia (MSG-A)

**Table 1** Crystallite size, microstrain, lattice parameters and magnetic parameter of  $\text{MgFe}_2\text{O}_4$  obtained by XRD and VSM

Synthesis method of $\text{MgFe}_2\text{O}_4$ NPs	CS (nm) (from XRD)	MS (%)	Lattice parameter ( $\text{\AA}$ )	$M_s$ (emu/g)	$M_r$ (emu/g)	Hc (Oe)
SG	4	0.0490	$a = 8.385$ (11)	5.392	48.02	7.076
MSG-A	13	0.1500	$a = 8.387$ (18)	9.936	3.038	103.1

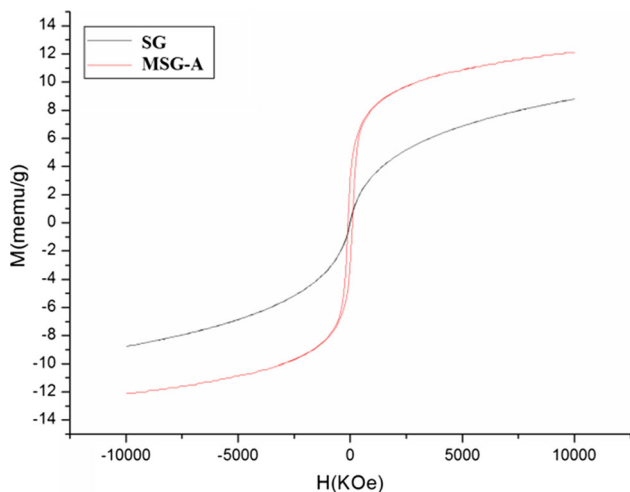


**Fig. 4** M-H hysteresis loops of MgFe<sub>2</sub>O<sub>4</sub> nanopowders prepared by SG and MSG-A methods

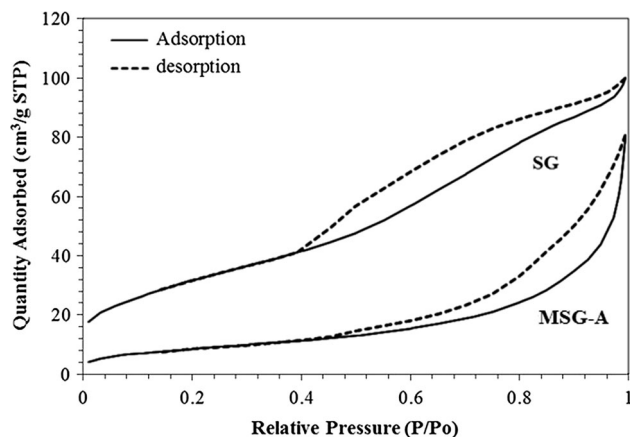


**Fig. 5** Adsorption-desorption isotherms of N<sub>2</sub> at 77 K of SG and MSG-A nanopowders

the nanopowders. The magnetic properties of spinel phases are known to be very sensitive depending on the synthesis conditions, particle size and the occupancy rate of Mg and Fe ions within tetrahedral (T), and octahedral (O) sites within the cubic crystal structure (Mg<sub>1-x</sub>Fe<sub>x</sub>)(Fe<sub>1-y</sub>Mg<sub>y</sub>)<sub>2</sub>, as *x* and *y* may vary considerably. This was reported for magnesium ferrite [16] and other ferrites such as Co-Zr-doped strontium hexaferrite SrCo<sub>x</sub>Zr<sub>x</sub>Fe<sub>(12-2x)</sub>O<sub>1</sub> [24] and Co<sub>0.5</sub>Mg<sub>0.5</sub>Cr<sub>x</sub>Fe<sub>2-x</sub>O<sub>4</sub> [25]. Similar results were also obtained in other systems such as ZnO nanoparticles [26].

Isotherm shape provides information on pore size, which is usually categorized as micropore, mesopore, or macropore. For instance, Fig. 5 illustrates the N<sub>2</sub> adsorption-desorption isotherms for SG and MSG-A nanopowders. It is clear that the N<sub>2</sub> adsorption-desorption isotherm of SG nanopowder exhibits a combination of type I and II shape, as per the classification of IUPAC for sorption isotherms [27], matching the specifications of a solid material rich in

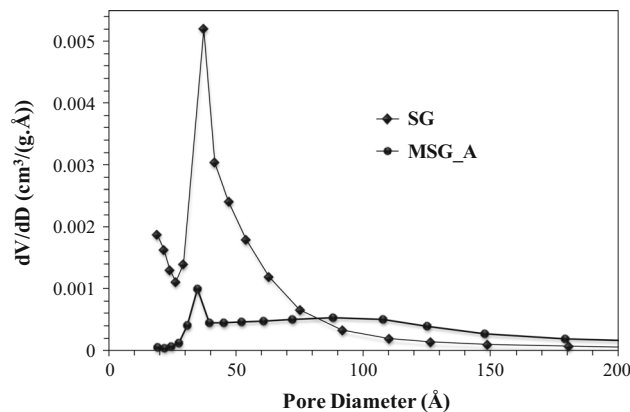


**Fig. 6** Pore size distribution of SG and MSG-A nanopowders

mesopores. The hysteresis loop of H2-type for SG material indicated a slit-shaped mesopores, similar to many nano-materials (i.e., as it can be seen in Fig. 6 of pore distribution and the calculated average pore diameter 45 Å in Table 2). However, the modified MSG-A nanopowder exhibits a sorption isotherm of type II, with a hysteresis loop of H4 type. At elevated relative pressure *P/P*<sub>0</sub>, the hysteresis of H4 type was due to the filling up of mesopores by capillary condensation, indicating a shape of pores that was flatter instead of cylindrical (average pore diameter 113 Å).

The BJH method was used for the determination of the pore size distribution. As shown in Fig. 6, the pore size distribution of SG nanopowder is narrow and do not exceed 50 Å with an average pore diameter of about 45 Å. It is obvious that the average pore diameter of the nanopowder prepared using the modified sol-gel method is increased, and the pore size distribution is well dispersed in the interval 45 to 200 Å.

Particle size, pore characteristics, and BET surface area are listed in Table 2. The surface area is significantly decreased from 115.3 to 31.6 m<sup>2</sup>/g by the modified method. The results showed also that the modified process increased the average diameter of pores (from 45 to 113 Å). This finding was in accordance with XRD results (Table 2) as well as SEM images (Fig. 4).

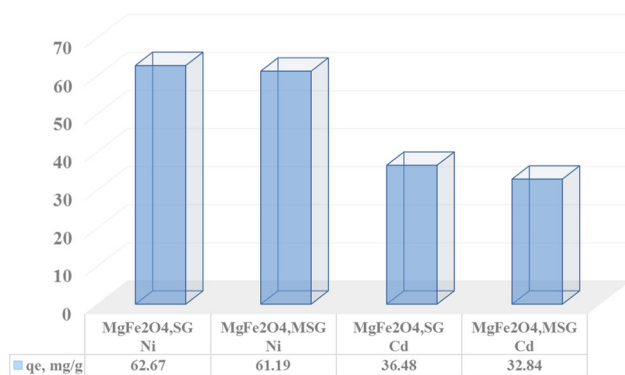
### 3.2 Adsorption capacity tests

The experiment of selective removal of (Cd(II) and Ni(II)) ions, which are well-known toxic heavy metals, was carried out at room temperature with a pH value fixed at 7.0 ± 0.2.

Figure 7 illustrates the experimental results of adsorption capacities of both heavy metals ions by both adsorbents, respectively. The figure showed clearly that the adsorption of both adsorbents for Ni(II) is higher than that for Cd(II) as the adsorption capacity of Ni(II) ions is about

**Table 2** Main characteristics of SG and MSG-A nanopowders

Synthesis method of MgFe <sub>2</sub> O <sub>4</sub> NPs	CS (nm) (from XRD)	Grain size (nm) (from FESEM)	Average pore diameter (Å)	Average pore volume (cm <sup>3</sup> g <sup>-1</sup> ) × 10 <sup>2</sup>	Surface BET (m <sup>2</sup> g <sup>-1</sup> )
SG	4	5–30	45.35	16.1	115.3
MSG-A	13	20–50	113.36	11.76	31.6

**Fig. 7** Ultimate adsorption capacities of toxic heavy metal (Ni and Cd) ions removal by SG and MSG-A nanopowders

62.67 and 61.2 mg g<sup>-1</sup> for MgFe<sub>2</sub>O<sub>4</sub> nanopowder, SG and MSG-A, while in the case of Cd(II) the values observed are 36.49 and 32.84 mg g<sup>-1</sup>, respectively. Although the surface area of SG sample is around four times higher than that of MSG-A, both samples showed a close adsorption rate. This can be explained as follows: the size of MSG-A NPs is four times larger than the size of SG NPs, in agreement with surface area, therefore, the smaller the particle size, the higher tendency of agglomeration (Fig. 8) because each NP can be considered as a “magnet” [28]. This will directly affect the available surface sites for the adsorption, leading to a relatively lower adsorption rate.

In this study, the synthesized MgFe<sub>2</sub>O<sub>4</sub> nanopowders with SG and MSG methods have shown a considerable adsorption capacity for the removal of Ni and Cd metals in comparison with other magnetic nanoabsorbents (Table 3). For example, in a previous study [29] on the removal of the same heavy metals using Ni-doped α-Fe<sub>2</sub>O<sub>3</sub> nanoparticles, the adsorption capacities were found to be lower for Ni(II) metal ions (about 42 mg g<sup>-1</sup>) using similar experimental parameters. It is essential to mention that the pH is one of the important influencing parameter during the adsorption experiments as several investigations showed that the maximum adsorption capacities can be obtained, during the removal of Cd(II) and Ni(II) by iron oxides nanoparticles, at pH values ranging from 5 to 8 [29]. On the other hand, Hu et al. [30] obtained relatively low adsorption

capacities for Ni(II) which was about 27 mg g<sup>-1</sup>, i.e., almost half the amount obtained in the present study. Subsequently, owing to the reason that the milled goethite is highly efficient for Ni(II) than the remaining metal ions, further experimental study will be devoted only to Ni(II) removal from aqueous solution. It is very important to note that Ni(II) is an oligo-element not very toxic at the natural state, but very toxic when bounded to synthesis products. Furthermore, MgFe<sub>2</sub>O<sub>4</sub> nanopowders have shown much higher adsorption capacity for Ni, than Fe ions [31] and some other iron oxides composites [32] that owned much lower adsorption capacities of Ni, i.e., 9.24 and 8 mg g<sup>-1</sup>, respectively, under very similar experimental conditions.

In the case of the adsorption of Cd metal ions, MgFe<sub>2</sub>O<sub>4</sub> powders adsorption capability was considerable too, while other adsorbant Ag-MWCNTs has slightly higher adsorption capacity of 54.94 mg g<sup>-1</sup> [34]. This can be explained by the higher temperature (39.5° C) and also the higher BET surface area 119.46 m<sup>2</sup>g<sup>-1</sup> that obtained for Ag-MWCNTs which confirms the correlation between the adsorption capacity and the BET surface area (Table 3).

## 4 Conclusion

MgFe<sub>2</sub>O<sub>4</sub> nanopowders have been successfully synthesized using different approaches and different reagents followed by calcination. X-ray diffraction analysis confirms that pure single spinel cubic phase is formed with crystallite size in the range from 3 to 15 nm. The calcined nanopowders reveal room temperature ferromagnetism (RTFM) having a saturation magnetization in the range 5.4–9.9 emu/g. The as-prepared nanopowders have shown potential applications in heavy metal removal from aqueous solution. SG and MSG-A MgFe<sub>2</sub>O<sub>4</sub> nanopowders were identified as efficient adsorbents for Cd and Ni metals from aqueous solutions. The obtained results revealed better affinity for the removal of Ni(II) than Cd(II). In the present investigation, the maximum adsorption capacity is tested. Nevertheless, this study will be enriched by performing further experiments to evaluate

**Fig. 8** Effect of agglomeration of SG and MSG-A nanopowders on the uptake of ions

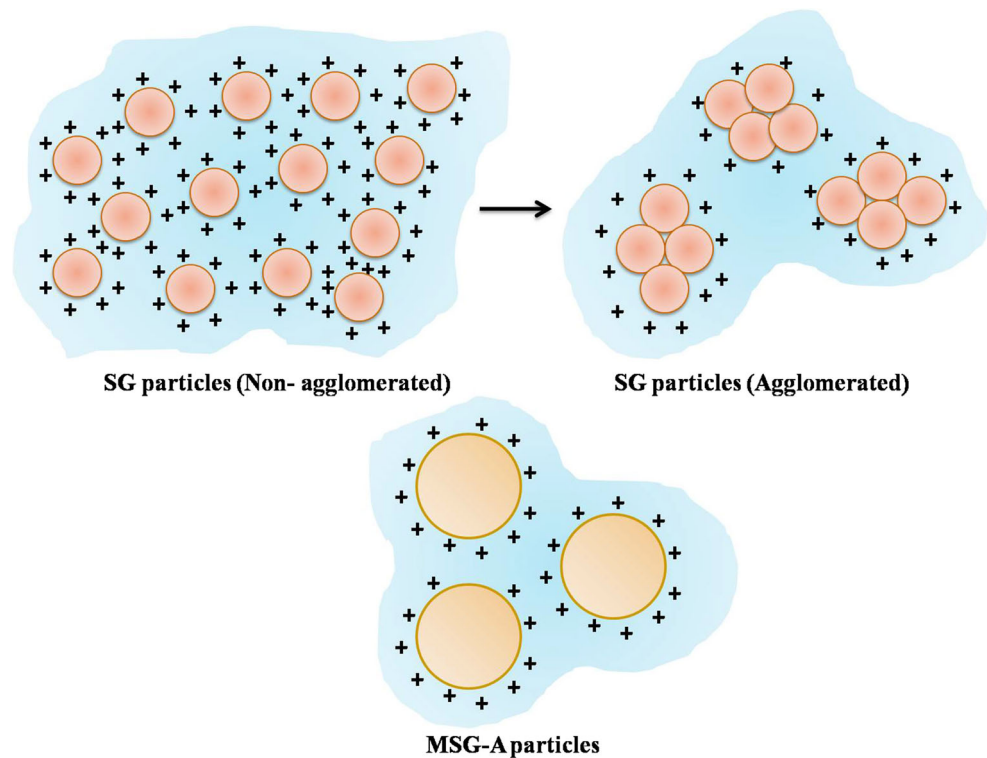


**Table 3** Comparison of MgFe<sub>2</sub>O<sub>4</sub> nanopowders with other adsorbents reported in the literature

Ion metal	Adsorbent	Temperature (°C)	PH	$q_{\max}$ (mg/g)	Ref
Ni(II)	MgFe <sub>2</sub> O <sub>4</sub> -SG	Room temperature	7	62.67	This study
	MgFe <sub>2</sub> O <sub>4</sub> -MSG-A	Room temperature	7	61.2	This study
	Ni-doped $\alpha$ -Fe <sub>2</sub> O <sub>3</sub>	Room temperature	7	42	[29]
	Fe	25		9.24	[31]
	iron oxide magnetic composites	25	6.4	8	[32]
	Maghmite $\alpha$ -Fe <sub>2</sub> O <sub>3</sub>		5–8	27	[30]
Cd (II)	MgFe <sub>2</sub> O <sub>4</sub> -SG	Room temperature	7	36.67	This study
	MgFe <sub>2</sub> O <sub>4</sub> -MSG-A	Room temperature	7	32.4	This study
	Iron oxide activated red	19.85	6	117.64	[33]
	Ni-doped Fe <sub>2</sub> O <sub>3</sub>	Room temperature	6.5	65.462	[29]
	Ag-MWCNTs	39.5	7	54.94	[34]
	Iron oxide	25	2–8	18.8	[35]

the kinetics, adsorption equilibrium and thermodynamic parameters of toxic heavy metal ions (Ni and Cd) by MgFe<sub>2</sub>O<sub>4</sub> nanopowders.

## References

- L.P. Lingamdinne, Y. Chang, J. Yang, J. Singh, E. Choi, M. Shiratani, J.R. Koduru, P. Attri, Biogenic reductive preparation of magnetic inverse spinel iron oxide nanoparticles for the adsorption removal of heavy metals. *Chem. Eng. J.* **307**, 74–84 (2017)
- T. Madrakian, A. Afkhami, B. Zadpour, M. Ahmadi, New synthetic mercaptoethylamino homopolymer-modified maghemite nanoparticles for effective removal of some heavy metal ions from aqueous solution. *J. Ind. Eng. Chem.* **21**, 1160–1166 (2015)
- W. Tang, Y. Su, Q. Li, S. Gao, J. Shang, Superparamagnetic magnesium ferrite nanoadsorbent for effective arsenic (III, V) removal and easy magnetic separation. *Water Res.* **47**, 3624–3634 (2013)
- J. Hu, I.M.C. Lo, G. Chen, Comparative study of various magnetic nanoparticles for Cr(VI) removal. *Sep. Purif. Technol.* **56**, 249–256 (2007)
- L. Zhao, X. Li, Q. Zhao, Z. Qu, D. Yuan, S. Liu, Xi Hu, G. Chen, Synthesis, characterization and adsorptive performance of MgFe<sub>2</sub>O<sub>4</sub> nanospheres for SO<sub>2</sub> removal. *J. Hazard. Mater.* **184**, 704–709 (2010)
- D. Chen, Y. Zhang, C. Tu, Preparation of high saturation magnetic MgFe<sub>2</sub>O<sub>4</sub> nanoparticles by microwave-assisted ball milling. *Mater. Lett.* **82**, 10–12 (2012)

7. S. Maensiri, M. Sangmanee, A. Wiengmoon, Magnesium ferrite ( $\text{MgFe}_2\text{O}_4$ ) nanostructures fabricated by electrospinning. *Nanoscale Res. Lett.* **4**, 221–228 (2009)
8. J. Fu, J. Zhang, C. Zhao, Y. Peng, X. Li, Y. He, Z. Zhang, X. Pan, N.J. Mellors, E. Xie, Solvent effect on electrospinning of nanotubes: the case of magnesium ferrite. *J. Alloys Compd.* **577**, 97–102 (2013)
9. M.G. Naseri, M.H.M. Ara, E.B. Saion, A. Shaari, Superparamagnetic magnesium ferrite nanoparticles fabricated by a simple, thermal-treatment method. *J. Magn. Magn. Mater.* **350**, 141–147 (2014)
10. Y. Shen, Q. Zhao, X. Li, Y. Hou, G. Chen, Surface photovoltage property of magnesium ferrite/hematite heterostructured hollow nanospheres prepared with one-pot strategy. *Colloids Surf. A: physicochem. Eng. Asp.* **403**, 35–40 (2012)
11. R. Ali, M.A. Khan, A. Mahmood, A.H. Chughtai, A. Sultan, M. Shahid, M. Ishaq, M.F. Warsi, Structural, magnetic and dielectric behavior of  $\text{Mg}_{1-x}\text{Ca}_x\text{Ni}_y\text{Fe}_{2-y}\text{O}_4$  nano-ferrites synthesized by the micro-emulsion method. *Ceram. Int.* **40**, 3841–3846 (2014)
12. T.K. Pathak, N.H. Vasoya, V.K. Lakhani, K.B. Modi, Structural and magnetic phase evolution study on needle-shaped nanoparticles of magnesium ferrite. *Ceram. Int.* **36**, 275–281 (2010)
13. G. Ferik, M. Drofenik, D. Lisjak, A. Hamler, Z. Jaglič, D. Makovec, Synthesis and characterization of  $\text{Mg}_{1-x}\text{Fe}_{2-2x}\text{Ti}_x\text{O}_4$  nanoparticles with an adjustable Curie point. *J. Magn. Magn. Mater.* **350**, 124–128 (2014)
14. B.C. Lippens, J.H. De Boer, Pore systems in catalysts.V. the t-method. *J. Catal.* **4**, 319–323 (1965)
15. E.P. Barrett, L.J. Joyner, P.H. Halenda, The determination of pore volume and area distribution on porous solids I: computation from nitrogen isotherms. *J. Am. Chem. Soc.* **73**, 373–380 (1951)
16. R. Tholkappian, K. Vishista, Combustion synthesis of Mg–Er ferrite nanoparticles: cation distribution and structural, optical, and magnetic properties. *Mater. Sci. Semicond. Process.* **40**, 631–642 (2015)
17. M. Sheykhan, H. Mohammadnejad, J. Akbari, A. Heydari, Superparamagnetic magnesium ferrite nanoparticles: a magnetically reusable and clean heterogeneous catalyst. *Tetrahedron Lett.* **53**, 2959–2964 (2012)
18. L. Khanna, N.K. Verma, Size-dependent magnetic properties of calcium ferrite nanoparticles. *J. Magn. Magn. Mater.* **336**, 1–7 (2013)
19. J. Wang, A. Sugawara-Narutaki, M. Fukao, T. Yokoi, A. Shimojima, T. Okubo, Two-phase synthesis of monodisperse silica nanospheres with amines or ammonia catalyst and their controlled self-assembly. *ACS Appl. Mater. Interfaces* **3**, 1538–1544 (2011)
20. H. Yuan, L. Zhang, M. Xu, X. Du, Effect of sol pH on microstructures, optical and magnetic properties of (Co, Fe)-codoped ZnO films synthesized by sol–gel method. *J. Alloy. Compd.* **651**, 571–577 (2015)
21. G.R. Kumar, K.V. Kumar, Y.C. Venudhar, Synthesis, structural and magnetic properties of copper substituted nickel ferrites by sol–gel method. *Mater. Sci. Appl.* **3**, 87–91 (2012)
22. C.P. Fernández, F.L. Zabetto, D. Garcia, R.H.G.A. Kiminami, In situ sol–gel co-synthesis under controlled pH and microwave sintering of PZT/ $\text{CoFe}_2\text{O}_4$  magnetoelectric composite ceramics. *Ceram. Int.* **42**, 3239–3249 (2016)
23. L.P. Singh, S.K. Agarwal, S.K. Bhattacharyya, U. Sharma, S. Ahalawat, Preparation of silica nanoparticles and its beneficial role in cementitious materials. *Nanomater. Nanotechnol.* **1**, 44–51 (2011)
24. S.K. Chawla, S.S. Meena, P. Kaur, R.K. Mudsainiyan, S.M. Yusuf, Effect of site preferences on structural and magnetic switching properties of CO–Zr doped strontium hexaferrite  $\text{SrCo}_x\text{Zr}_x\text{Fe}_{(12-2x)}\text{O}_{19}$ . *J. Magn. Magn. Mater.* **378**, 84–91 (2015)
25. M.V. Chaudhari, S.E. Shirsath, A.B. Kadam, R.H. Kadam, S.B. Shelke, D.R. Mane, Site occupancies of Co–Mg–Cr–Fe ions and their impact on the properties of  $\text{Co}_{0.5}\text{Mg}_{0.5}\text{Cr}_x\text{Fe}_{2-x}\text{O}_4$ . *J. Alloy. Compd.* **552**, 443–450 (2013)
26. Ö. Altıntaş Yıldırım, C. Durucan, Room temperature synthesis of Cuincorporated ZnO nanoparticles with room temperature ferromagnetic activity: structural, optical and magnetic characterization. *Ceramics International* (2015), <http://dx.doi.org/10.1016/j.ceramint.2015.10.113>
27. Q.Q. Miao, Y.M. Tang, J. Xu, X.P. Liu, L. Xiao, Q.H. Chen, Activated carbon prepared from soybean straw for phenol adsorption. *J. Taiwan Inst. Chem. Eng.* **44**(3), 458–465 (2013)
28. M. Kaur, N. Kaur, K. Jeet, P. Kaur,  $\text{MgFe}_2\text{O}_4$  nanoparticles loaded on activated charcoal for effective removal of Cr(VI)—A novel approach. *Ceram. Int.* **41**, 13739–13750 (2015)
29. O.M. Lemine, I. Ghiloufi, M. Bououdina, L. Khezami, M. Ould, M.O. M'hamed, A.T. Hassan, Nanocrystalline Ni doped  $\alpha\text{-Fe}_2\text{O}_3$  for adsorption of metals from aqueous solution. *J. Alloys Compd.* **588**, 592–595 (2014)
30. J. Hu, G. Chen, I.M.C. Lo, Selective removal of heavy metals from industrial wastewater using maghemite nanoparticle: performance and mechanisms. *J. Environ. Eng.* **132**(7), 709–715 (2006)
31. C. Zhou, T. Li, J. Liu, J. Wang, G. Liu, Synthesis, characterization and aging study of kaolinite-supported zero-valent iron nanoparticles and its application for Ni(II) adsorption. *Mater. Res. Bull.* **60**, 421–432 (2014)
32. C. Chen, J. Hu, D. Shao, J. Li, X. Wang, Adsorption behavior of multiwall carbon nanotube/iron oxide magnetic composites for Ni(II) and Sr(II). *J. Hazard. Mater.* **164**, 923–928 (2009)
33. T.A. Khan, S.A. Chaudhry, I. Ali, Equilibrium uptake, isotherm and kinetic studies of Cd(II) adsorption onto iron oxide activated red mud from aqueous solution. *J. Mol. Liq.* **202**, 165–175 (2015)
34. D.K.V. Ramana, J.S. Yu, K. Seshiah, Silver nanoparticles deposited multiwalled carbon nanotubes for removal of Cu(II) and Cd(II) from water: surface, kinetic, equilibrium, and thermal adsorption properties. *Chem. Eng. J.* **223**, 806–815 (2013)
35. J. Gong, L. Chen, G. Zeng, F. Long, J. Deng, Q. Niu, X. He, Shellac-coated iron oxide nanoparticles for removal of cadmium(II) ions from aqueous solution. *J. Environ. Sci.* **7**, 1165–1173 (2012)